# Towards a numerical multi-fidelity strategy for unsteady aerodynamics studies of reusable launch vehicles: Application to Ariane Next

*P. E. Weiss* and *S. Deck*
*ONERA - The French Aerospace Lab, F-92190, Meudon, France*

Reusable launch vehicles imply the use of innovative numerical multi-fidelity strategies to allow the proper prediction of the related unsteady aerodynamic properties. In that view, a numerical workflow denoted as Zonal Immersed Boundary Conditions (ZIBC) has been developed[20,32] and successfully applied to full space launcher models namely Ariane 5[32] as well as Ariane 6 PPH.[33] Such a framework permits a global survey of the timeline of the flight of a sub-scale Ariane Next configuration with a particular focus on the descent based on URANS and ZDES computations. In practice, the main cylindrical body with aft and forward axisymmetric skirts are modelled using a classical body-fitted (BF) approach. All other technological details are taken into account by the local introduction of source terms (namely immersed boundary conditions (IBC)) as in Weiss and Deck[32] or Manueco *et al.*[17] The robustness and the accuracy of the approach provides a rapid overview of the instantaneous coherent structures in the turbulent flow. The salient features of the flow topology are also depicted on the basis of first-order statistics for cases with different physical conditions from the transonic to the supersonic regimes at Mach numbers $M_0$ equal to 0.8 and 2 with and without incidence. Finally, the multi-fidelity strategy provides a first glimpse into the spatial organisation of the unsteady flow using ZDES mode 2 (2020)[8] computations.

## 1. Introduction

The rise of the NewSpace paradigm and the objective of halving the costs of European launchers in 2030s for the next generation of Ariane Launchers[5] come with a growing need for reactivity and accuracy in the design of reusable launchers.[2,15,18] Simulation tools have reached a sufficient level of maturity to allow the reproduction and the prediction of unsteady aerodynamic phenomena on space vehicles.[3,32] Such a statement is well-illustrated by the long history of studies dedicated to the investigation of the buffeting phenomenom[4,9,11,28,34] following Ariane 5 flight 157 as recently reminded by Saile *et al.*[27] In this context, the present study gives an example of the use of CFD as a multi-fidelity strategy to rapidly evidence instabilities and anticipate the occurrence of unsteady loads potentially leading to strong disturbances such as the buffeting phenomenon but also ovalization of nozzles[23] or any unsteadiness that may affect the stability of the launch vehicle.

The objective is here to demonstrate the capacity of the ZIBC (Zonal Immersed Boundary Conditions) approach[16,20,32] coupling a turbulence model (first URANS (Unsteady Reynolds-Averaged Navier-Stokes) and then ZDES (Zonal Detached Eddy Simulation)) and IBC (Immersed Boundary Conditions) to identify and analyse the flow physics of the unsteady flow phenomena with a limited amount of time devoted to the building of the numerical test case. The first part of the paper details the ZIBC methodology based on URANS with a Spalart-Allmaras model applied to one of the reusable launch vehicle concept that paves the way for the next generation of Ariane Launchers. Then, the first results issued from the ZDES allow to evidence the different instantaneous characteristics of the flow field for the two Mach numbers of interest namely 0.8 and 1.94 which would not have been possible with a steady RANS approach.

TOWARDS A NUMERICAL MULTI-FIDELITY STRATEGY FOR UNSTEADY AERODYNAMICS STUDIES OF
REUSABLE LAUNCH VEHICLES: APPLICATION TO ARIANE NEXT

## 2. Description of the test case

The present configuration corresponds to a next generation design of a reusable launch vehicle investigated during the
return phase. A global view of this reusable space launcher is provided in Figure 1. Such a configuration is made of
a single cylindrical main stage with a diameter $D = 0.108$ m which constitutes the reference length $L_{\text{ref}}$ and several
technological details that are visible in Figure 1. Attached to the central body one can find from top to bottom: a hemi-
spherical cap on a ring, four deployed grid fins and four stowed landing legs. At the afterbody base, a single nozzle is
surrounded by eight nozzles distributed azimuthally. Then, the full length $L_{\text{NT}}$ from nose to tail of the space launcher
is approximately equal to $8.1D$ while the cylindrical body alone is 7.9 diameters long.

Among the numerous configurations in return phase that have been assessed for different Mach numbers, two
are considered in the present paper in the transonic and supersonic regimes namely $M_\infty = 0.8$ and $M_\infty = 1.94$ that are
denoted in the following as M08 and M194, respectively. For M08, the stagnation pressure $Pi$ is equal to 106103 Pa
and the stagnation temperature $Ti$ is set to 318 K. For M194, $Pi = 172421$ Pa and $Ti = 403$ K. The configuration is
either inclined by an angle $\alpha = 10°$ or has no incidence so that the flow arrives from the bottom of the engine bay as
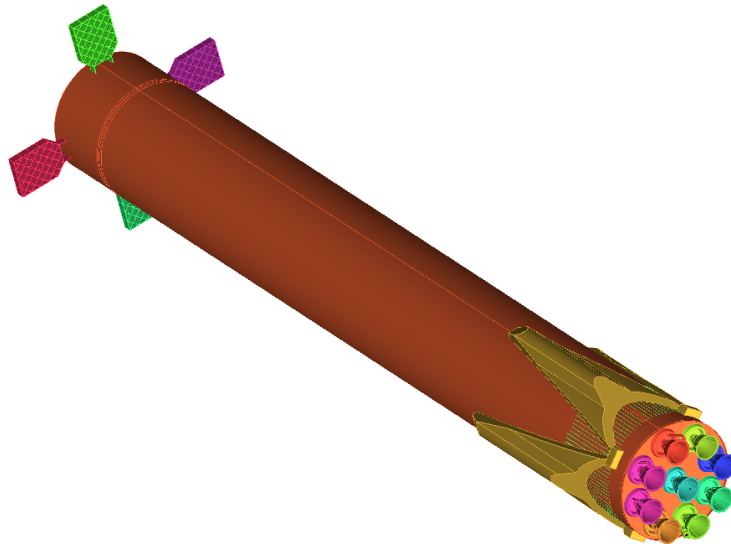represented in Figure 2.



Figure 1: Geometry of the reusable launch vehicle concept.



Figure 2: Flow direction with respect to the vehicle for the two angles of attack $\alpha = 0°$ and $\alpha = 10°$.

## 3. Mesh properties

The aforementioned freestream conditions lead to a classical first cell size in the wall normal direction $y^+ = 1$ for the two Mach numbers. The lowest cell size is retained allowing to make a common mesh for both cases. A structured multi-block grid is built around the smooth version of the configuration (i.e. limited to the main stage without any technological details). The generation of the grid is based on an O-H topology depicted in figure 3.
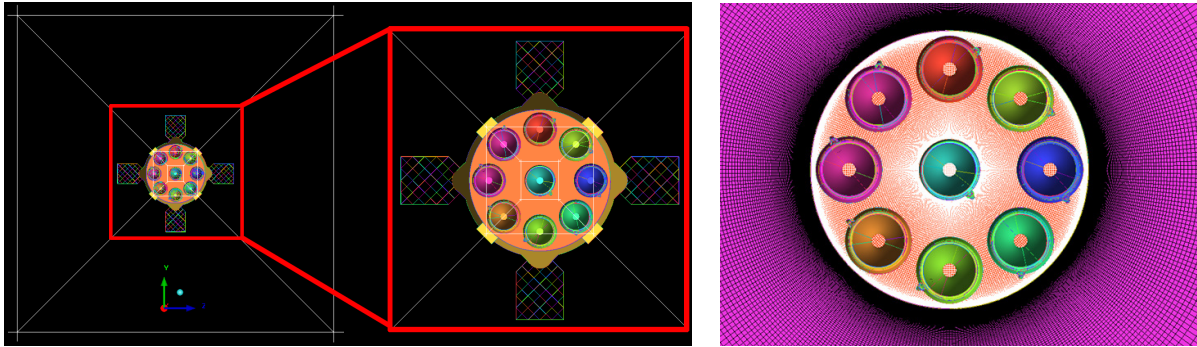


Figure 3: Rear view of the O-H topology (left) surrounding the main stage, the four grid fins and the nine nozzles in the propulsive bay along with the corresponding mesh at the wall and in the mesh (right).

The resulting mesh constitutes the background grid for the introduction of Immersed Boundary Conditions (IBC) that are described in the next section. Such a topology is designed to avoid singularity problems near the axes.
The whole computational domain consists in a cylinder with a circular section as shown in figure 4. Its characteristic sizes are willingly high compared to the diameter $D$ of the main stage base to avoid any reflections of spurious numerical waves. In practice, the length of the computational domain is approximately equal to $410D$ and its diameter equals $400D$ which permits a shift between the area of interest and the boundary of the computational domain equal to $200D$ in the three directions of space.
Knowing the grid refinement in the azimuthal direction often rules the spatial organisation for the azimuthal modes,[9,31,34] the number of points must be chosen accordingly. As a consequence, the smooth configuration (without any technological details) clusters 360 points in the azimuthal direction providing 1 degree between two longitudinal planes.
The neighbourhood of the main technological details (e.g. grid fins, landing legs and nozzles) is then particularly refined in the streamwise and longitudinal directions to allow an accurate prediction of phenomena such as mixing layers, wakes or shock waves as shown in Figure 5. For the cases with an angle of incidence $\alpha = 10°$, the topology of the mesh, the anisotropy and the asymmetry of the cells (characterized by their skewness) are inclined accordingly as illustrated in Figure 6. In the end, the mesh is made up with 53 blocks and contains $37 \times 10^6$ points for the URANS computations and $245 \times 10^6$ points for the ZDES ones.
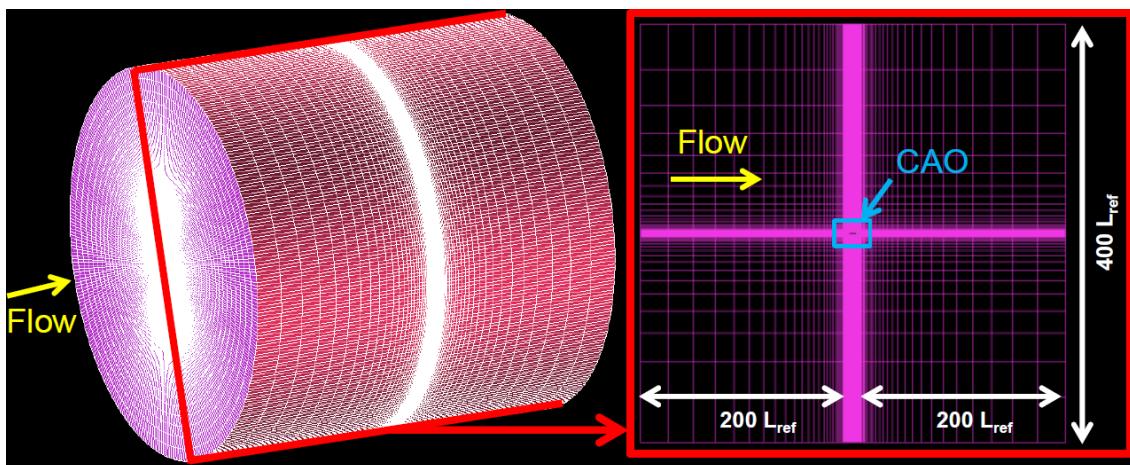


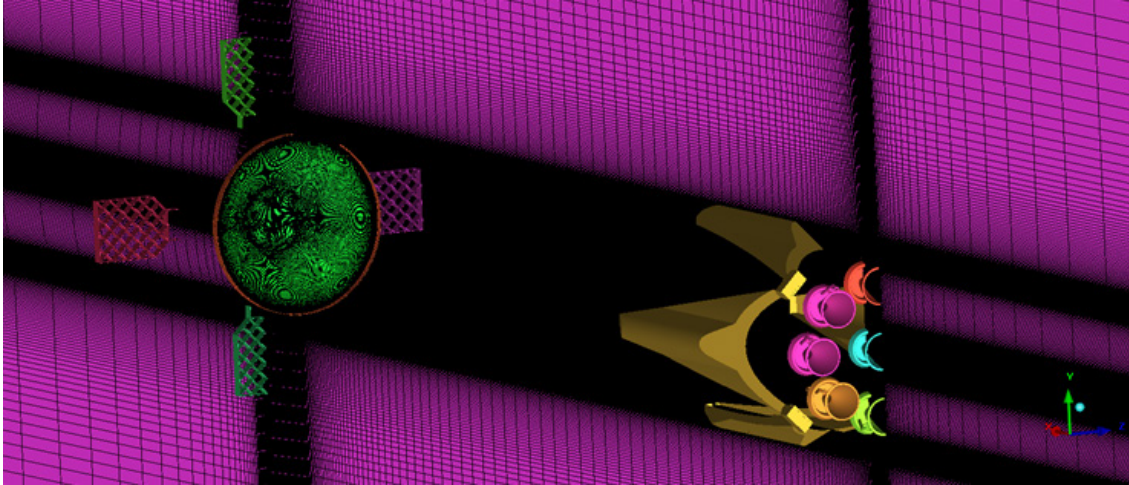Figure 4: Global view of the whole computational domain.

Figure 5: Longitudinal cut of the background grid for the case with no incidence.
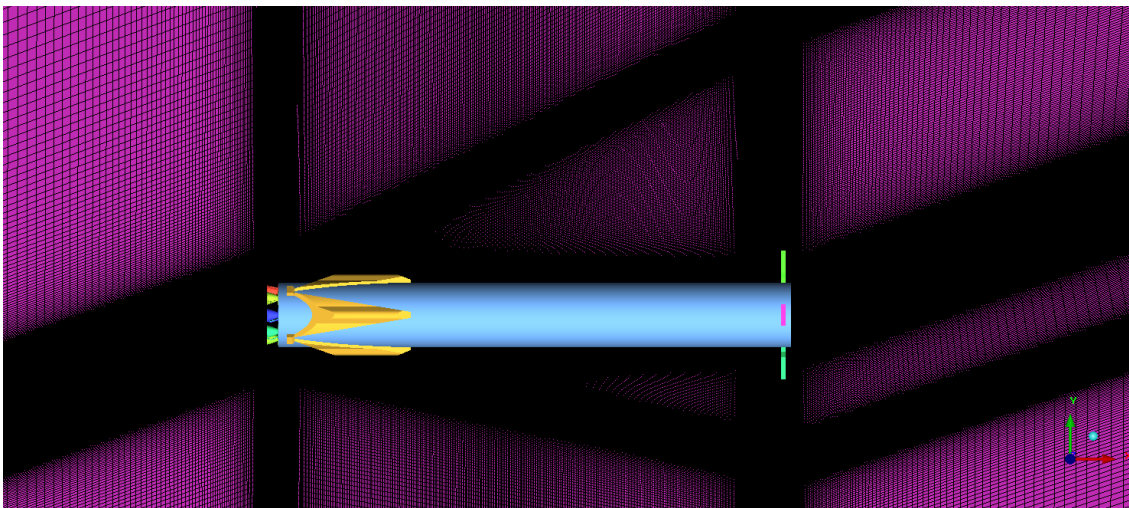


Figure 6: Mesh for the case with an angle of incidence $\alpha = 10°$.

# 4. Numerical set-up: ZIBC strategy



(a) Elements modelled with a body-fitted approach (grey) and Immersed Boundary Conditions (yellow)

(b) Iso-contours of the distance to the wall $d_w$ and iso-surface (red) of the technological details tag.
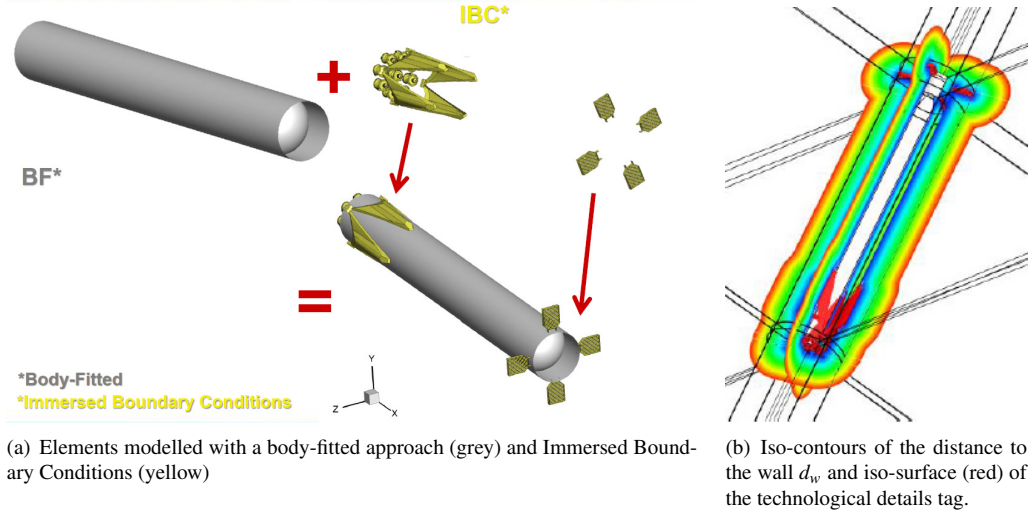
Figure 7: Illustration of the ZIBC strategy to take into account the technological details.

The approach used to take into account complex technological details is the immersed boundary method whereas the main stage is represented by a body fitted mesh which corresponds to the previously described background grid (see Figure 7(a)). Such a method consists in adding body forces in a continuous or discrete manner to mimic classical boundary conditions (e.g. adiabatic or isothermal walls, slip or no-slip conditions, porosity, etc ...). Since the first introduction of the immersed boundary method by Peskin[25] in 1972, the choice of either a continuous or a discrete form of the body forces highly depends on the application at stake (see e.g. Mittal and Iaccarino[19]). For instance, a continuous forcing function introduced in the governing equations before the discretization step appeared more adapted to elastic boundaries.[25,26] Given the rigid bodies considered in the present study and following the conclusions in Goldstein *et al.*[12] and Lai and Peskin,[14] a discrete forcing function has been privileged.

In the present work the continuous form of the compressible Navier-Stokes equations including the ZDES and IBC source terms is summarised. Then, for the sake of brevity, the discrete version of this system, which is implemented in practice, can be found in details in Weiss and Deck[32] for the finite volume approach in the same spirit as in Mohd-Yusof[21] for a spectral approach or Verzicco *et al.*[30] and Fadlun *et al.*[10] for a finite-difference-based LES. The source terms related to the ZDES and the IBC are clearly highlighted in the description of the formulation by the notations $\mathbf{T}_{\mathbf{ZDES}}^{(1)}$ and $\mathbf{T}_{\mathbf{IBC}}^{(2)}$, respectively.

The underlying notion existing behind the coupling between a hybrid RANS/LES method such as ZDES and IBC is a combination of source terms. Writing the integral form of the governing equations, these source terms can be clearly exhibited. In the frame of a finite volume approach, let us consider a finite volume $\Omega$ enclosed by a surface $\partial\Omega$ with $\mathbf{n}$ the normal surface vector associated to $d\Sigma$. The Navier-Stokes equations can be written as follows:

$$\frac{\partial}{\partial t}\int_\Omega \mathbf{W}d\Omega + \oint_{\partial\Omega}(\mathbf{F_c}[\mathbf{W}] - \mathbf{F_d}[\mathbf{W}, \nabla\mathbf{W}]).\mathbf{n}d\Sigma = \int_\Omega \mathbf{T}(\mathbf{W}, \nabla\mathbf{W})\,d\Omega \tag{1}$$

where $\mathbf{W}$ is the conservative variable vector, $\mathbf{F_c}$ and $\mathbf{F_d}$ contain the convective and diffusive fluxes respectively and $\mathbf{T} = \mathbf{T}_{\mathbf{ZDES}}^{(1)} + \mathbf{T}_{\mathbf{IBC}}^{(2)}$ denotes the source term.

In the above-mentioned equation, $\mathbf{T}_{\mathbf{IBC}}^{(2)} = \alpha_{IBC} \times \mathbf{f_{IBC}}(\mathbf{W}, \nabla\mathbf{W})$ with $\alpha_{IBC} = 0$ or $1$ depending on whether the considered area is fluid or solid, respectively and $\mathbf{f_{IBC}}$, the forcing function prescribed to obtain the targeted physical properties of the immersed boundaries.

It can be noticed that a tagging procedure has to be performed distinguishing solid cells from fluid cells. This permits to obtain values of *tagibc* which corresponds to $\alpha_{IBC}$ in the discrete form of the source term $\mathbf{T}_{\mathbf{IBC}}^{(2)}$ and acts as a sensor that reads as:

$$tagibc = \begin{cases} 1 & \text{if the cell center is inside the immersed object} \\ 0 & \text{if the cell center is outside the immersed object} \end{cases} \tag{2}$$

A major difference exists between $\alpha_{IBC}$ and *tagibc*. $\alpha_{IBC}$ can be equal to 1 in a part of a cell and equal to 0 in the

TOWARDS A NUMERICAL MULTI-FIDELITY STRATEGY FOR UNSTEADY AERODYNAMICS STUDIES OF
REUSABLE LAUNCH VEHICLES: APPLICATION TO ARIANE NEXT

remaining volume of the same cell. On the contrary, each cell has a value of 0 or 1 for the marker *tagibc*.

In the frame of the Spalart-Allmaras model[29] used in the URANS approach and on which is based ZDES, the
accurate calculation of the distance to the wall $d_w$ is crucial.

As mentioned before, the use of immersed boundary conditions requires a pre-processing step to distinguish
fluid cells (i.e. outside the bodies) from solid cells (i.e. inside the bodies) using a raytracing algorithm such as the
one described by O'Rourke[22] from the knowledge of the surface of the technological details which can be made of
triangles as in a STL (STereo-Lithography) CAD file. Following the immersion of the object, an update of the wall
distance computation has to be performed when a turbulence model needs it (e.g. the Spalart-Allmaras model). First,
the distance to the wall $d_w^B$ of the object is computed. During this procedure, the cells inside the geometry are treated
as if they were infinitely far from the body. Such a treatment permits to avoid the destruction term in the transport
equation of the pseudo-eddy viscosity returns negative values for the pseudo-eddy viscosity.[20] In practice, the 'infinite'
distance is explicitly set in meters to $10^9$ m. Then, the algorithm considers the former wall distances $d_w^A$ corresponding
to the geometry without technological detail and modelled with classical boundary conditions. Finally, the minimum
between the two distances $d_w^A$ and $d_w^B$ ($d_w = min(d_w^A, d_w^B)$) is preserved and provides the final distance-to-the-wall for the
whole configuration.

The selected method consists in a modified approach by Deck[6,7] of the original DES97 (Spalart *et al.*[29]), named
Zonal Detached Eddy Simulation (ZDES).

This multi-resolution approach covers the full range of modelling from RANS to LES and aims at treating all
classes of flow problems in a single model. To do so, RANS and DES zones are chosen individually. In RANS regions,
the model is enforced to behave as a RANS model while in the DES regions, the model can switch from the RANS
mode to the LES mode thanks to the following equation:

$$\tilde{d} = \begin{cases} d_w, & mode = 0 \\ \tilde{d}_{DES}^I, & mode = 1 \\ \tilde{d}_{DES}^{II}, & mode = 2 \\ \tilde{d}_{DES}^{III}, & mode = 3 \end{cases} \tag{3}$$

where $\tilde{d}$ stands for the new definition of the hybrid length scale chosen as a function of the nature of the separation.
$d_w$ corresponds to the closest distance to the wall. The definitions of $\tilde{d}_{DES}^I$, $\tilde{d}_{DES}^{II}$ and $\tilde{d}_{DES}^{III}$ can be found in Deck.[7] Its
advantage lies in the fact that the user can refine the grid in the areas of interest without spoiling the properties of the
boundary layer upstream or downstream the separation. The ZDES formulation differs from the DDES and DES97
ones given the functions close to the wall of the RANS model are explicitly nullified in LES mode. The sub-grid length
scale is provided by the cubic root of the volume similarly as in classical sub-grid scale models. In practice, the ZDES
rapidly switches into LES, limiting the extension to the grey zone responsible for the delay of the formation of the
instabilities.
In the frame of the use of Immersed Boundary Conditions, the most automated mode of ZDES namely mode 2 is
well-adapted to predict separations for configurations with high pressure and velocity fluctuation downstream. In the
present study, the most recent version of the method is used namely ZDES mode 2 (2020)[8] where the switch between
RANS and LES zones is set dynamically by the model itself.

We have implemented the original IB method (i.e. direct forcing) in two industrial flow solvers namely FLU3M[13]
and ONERA's elsA software.[1] Both codes are based on second-order accurate time and space schemes. The calcu-
lations presented in this paper are performed with the FLU3M code. The time steps for the URANS and ZDES
computations are $\Delta t = 10^{-5}$ s and $\Delta t = 10^{-6}$ s, respectively. Time accuracy of the calculation was checked during
the inner iteration process.[24] The URANS and ZDES simulations were realised on 84 and 504 Broadwell cores, re-
spectively. The preprocessing needed by the IBC to distinguish mesh cells with a fluid or solid tag is realized by the
external program RAYTRACER3D[20] for FLU3M.

# 5. Time-averaged aerodynamic characterization: URANS computations



(a) $M_0 = 0.8$ - $\alpha = 0°$

(b) $M_0 = 0.8$ - $\alpha = 10°$

(c) $M_0 = 1.94$ - $\alpha = 0°$

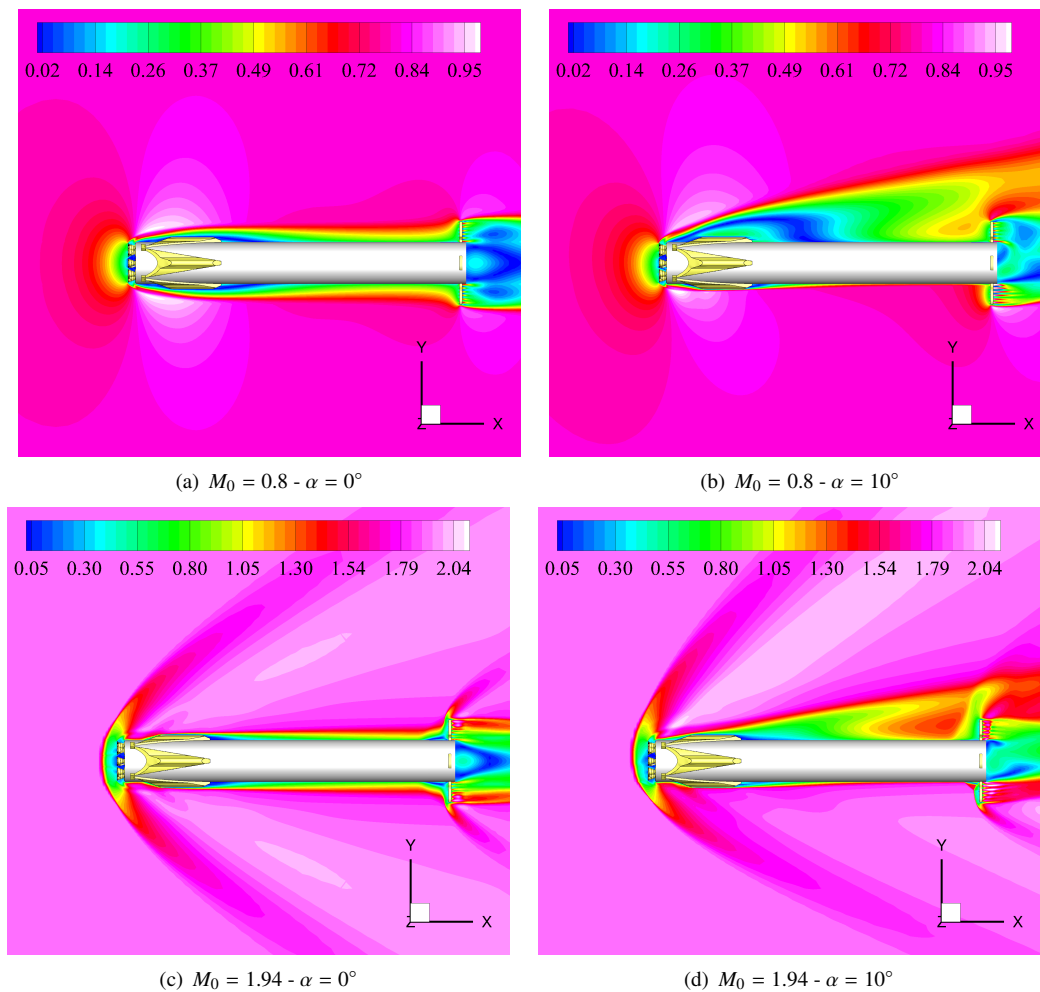(d) $M_0 = 1.94$ - $\alpha = 10°$

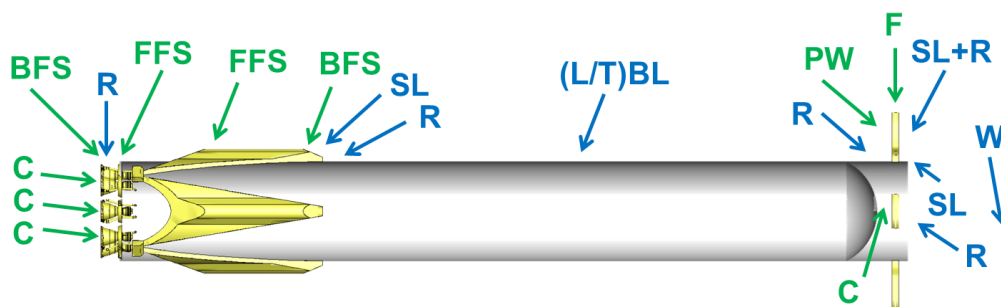Figure 8: Global view of iso-contours of the mean Mach number in a XY-plane.



Figure 9: Decomposition of the global configuration into academic flow cases (green) and related physical phenomena (blue).

TOWARDS A NUMERICAL MULTI-FIDELITY STRATEGY FOR UNSTEADY AERODYNAMICS STUDIES OF
REUSABLE LAUNCH VEHICLES: APPLICATION TO ARIANE NEXT

The first step of our multi-fidelity strategy consists in a series of preliminary URANS computations for both
Mach numbers and both angles of incidence. The salient features of the mean flow topology are clearly visible in
Figures 8 and 10 exhibiting the mean Mach number $M$ and mean pressure coefficient $Cp$ iso-contours, respectively.

Considering the geometrical complexity of the reusable launch vehicle configuration leading to a flow made up
with several interactions, a decomposition into academic configurations is proposed in Figure 9 in a non-exhaustive
way:

- BFS: *Backward Facing Step*

- FFS: *Forward Facing Step*

- F: *Fence*

- C: *Cavity*

- PW: *Porous-like Wall*


and related to expected physical phenomena:


- (L/T)BL : *(Laminar/Turbulent) Boundary Layer*

- SL: *Shear Layer*

- R: *Recirculation Zone*

- W: *Wake*

- The occurrence of shock waves and expansion fans depends on the flow regime and are willingly not indicated
  in Figure 9


Detailed views are also proposed for the mean Mach number and mean pressure coefficient in the grid fin area
(see Figures 11 and 12) and in the engine bay region (see Figures 13 and 14).

TOWARDS A NUMERICAL MULTI-FIDELITY STRATEGY FOR UNSTEADY AERODYNAMICS STUDIES OF
REUSABLE LAUNCH VEHICLES: APPLICATION TO ARIANE NEXT

(a) $M_0 = 0.8 - \alpha = 0°$

(b) $M_0 = 0.8 - \alpha = 10°$

(c) $M_0 = 1.94 - \alpha = 0°$

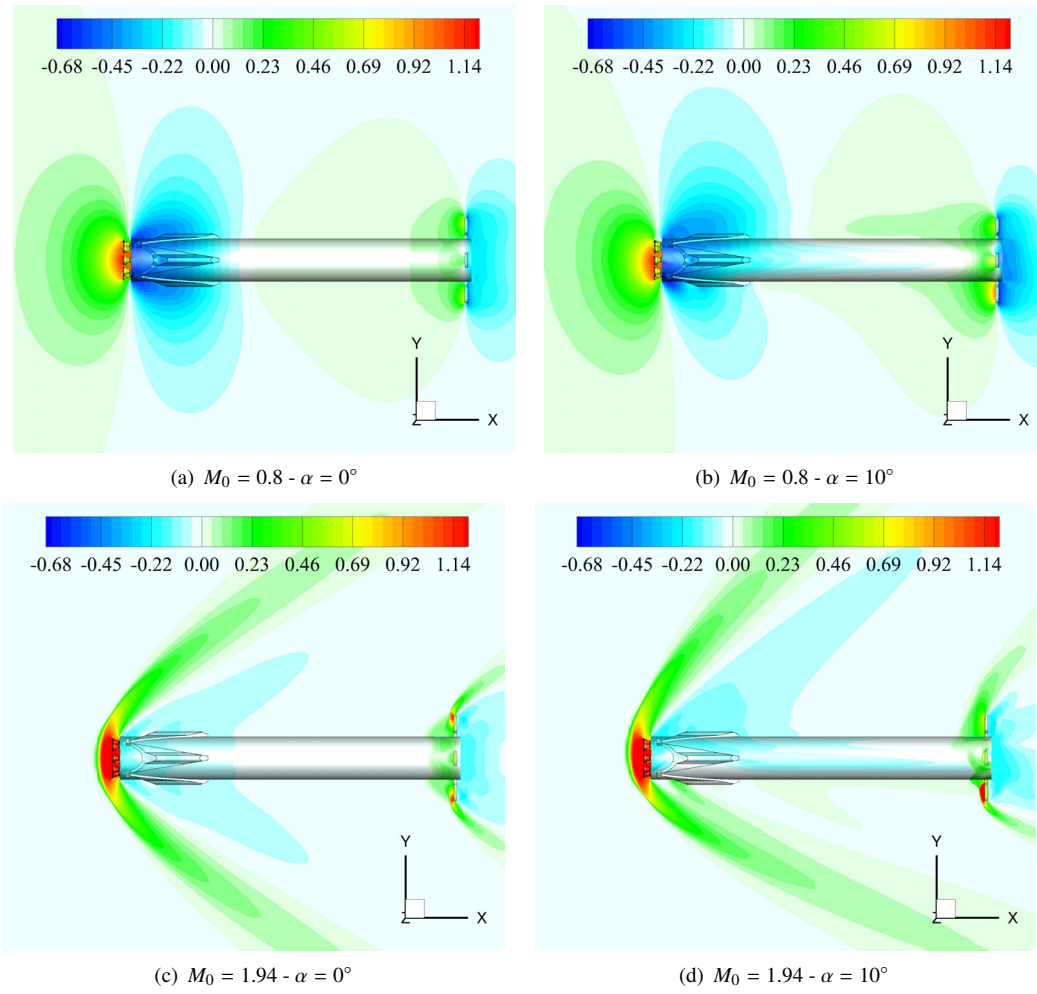(d) $M_0 = 1.94 - \alpha = 10°$

Figure 10: Global view of iso-contours of the mean pressure coefficient in a XY-plane.

TOWARDS A NUMERICAL MULTI-FIDELITY STRATEGY FOR UNSTEADY AERODYNAMICS STUDIES OF
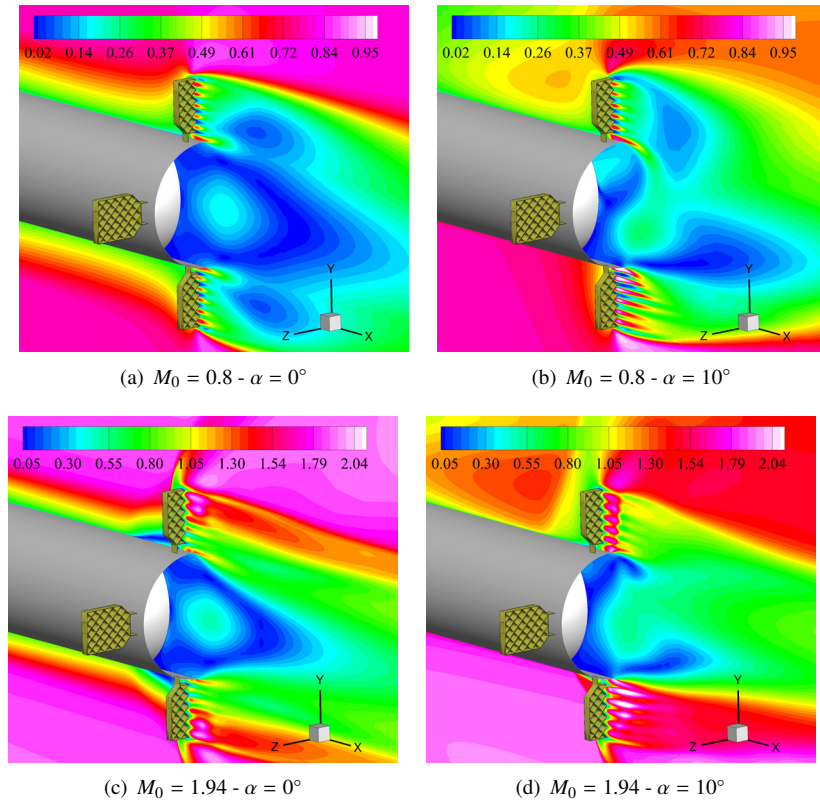REUSABLE LAUNCH VEHICLES: APPLICATION TO ARIANE NEXT

(a) $M_0 = 0.8 - \alpha = 0°$

(b) $M_0 = 0.8 - \alpha = 10°$

(c) $M_0 = 1.94 - \alpha = 0°$

(d) $M_0 = 1.94 - \alpha = 10°$

Figure 11: Mean Mach number iso-contours in a XY-plane in the grid fins area.

(a) $M_0 = 0.8 - \alpha = 0°$

(b) $M_0 = 0.8 - \alpha = 10°$

(c) $M_0 = 1.94 - \alpha = 0°$

(d) $M_0 = 1.94 - \alpha = 10°$
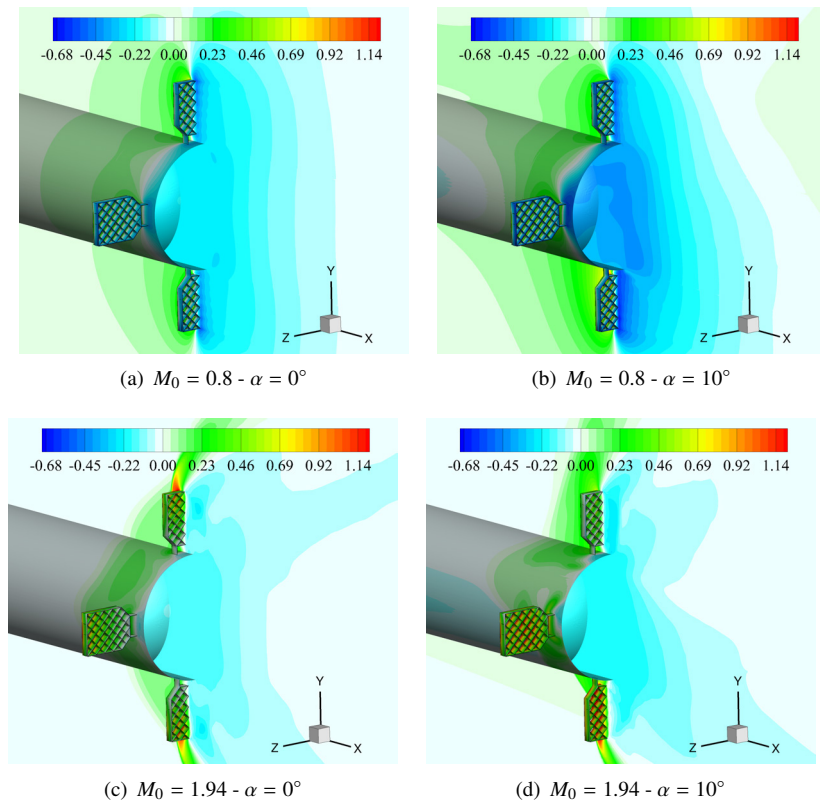
Figure 12: Mean pressure coefficient iso-contours in a XY-plane in the grid fins area.

(a) $M_0 = 0.8 - \alpha = 0°$

(b) $M_0 = 0.8 - \alpha = 10°$

(c) $M_0 = 1.94 - \alpha = 0°$

(d) $M_0 = 1.94 - \alpha = 10°$

Figure 13: Mean Mach number iso-contours in a XY-plane in the engine bay area.



(a) $M_0 = 0.8 - \alpha = 0°$

(b) $M_0 = 0.8 - \alpha = 10°$

(c) $M_0 = 1.94 - \alpha = 0°$

(d) $M_0 = 1.94 - \alpha = 10°$

Figure 14: Mean pressure coefficient in a XY-plane in the engine bay area.

TOWARDS A NUMERICAL MULTI-FIDELITY STRATEGY FOR UNSTEADY AERODYNAMICS STUDIES OF
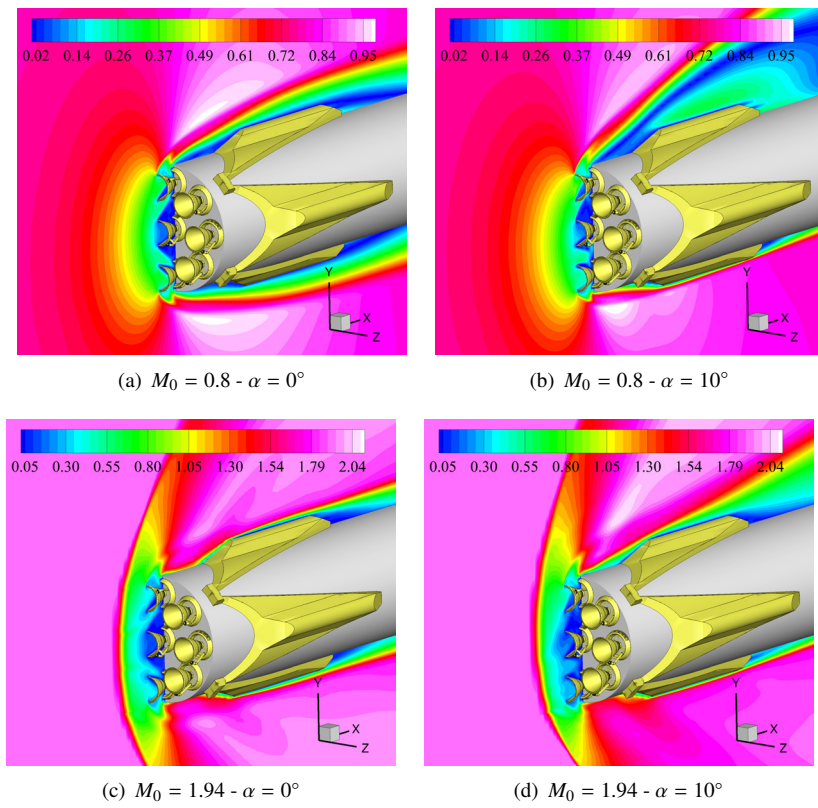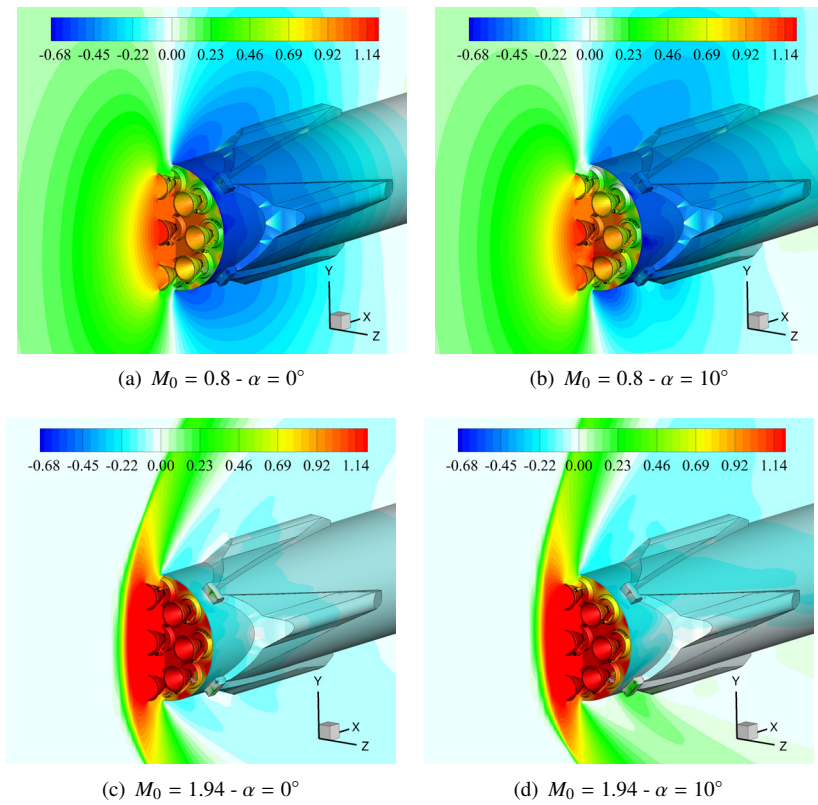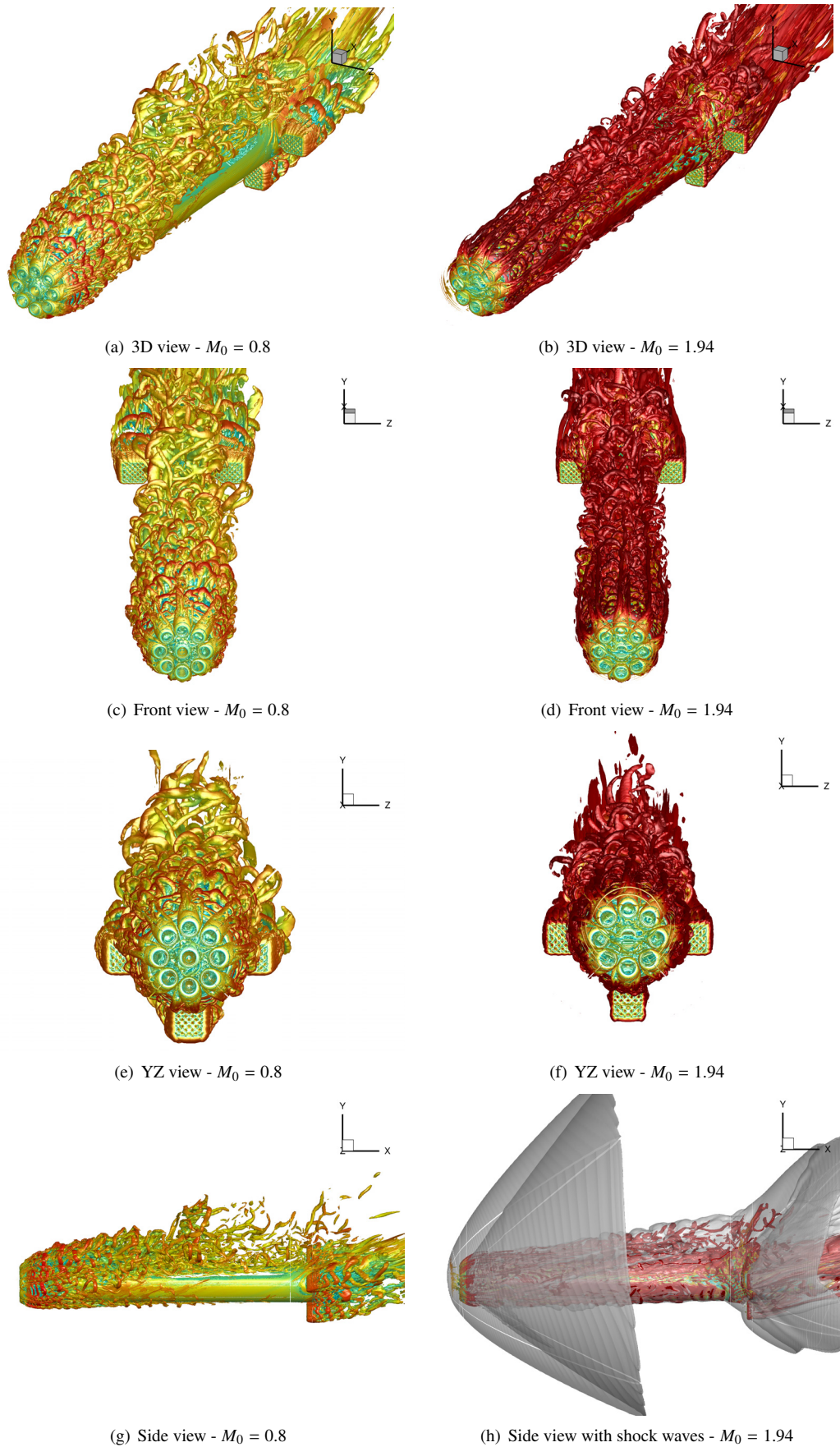REUSABLE LAUNCH VEHICLES: APPLICATION TO ARIANE NEXT



(a) 3D view - $M_0 = 0.8$

(b) 3D view - $M_0 = 1.94$

(c) Front view - $M_0 = 0.8$

(d) Front view - $M_0 = 1.94$

(e) YZ view - $M_0 = 0.8$

(f) YZ view - $M_0 = 1.94$

(g) Side view - $M_0 = 0.8$

(h) Side view with shock waves - $M_0 = 1.94$

Figure 15: Coherent structures (iso-surface of the dimensionless $Q^*$ criterion coloured by the streamwise velocity component) obtained with a ZDES computation of an Ariane Next case at $M_0 = 0.80$ (left) and $M_0 = 1.94$ (right) and $\alpha = 10°$ using the ZIBC framework.

## 6. Multi-scale resolution of the turbulent flow field: first ZDES results

In the previous URANS study, the observed asymmetry of the flow field suggests the potential occurrence of loads that could be higher than for the case with no incidence. Following the spirit of the present multi-fidelity approach and to go further in the observation of the turbulent field, ZDES mode 2 (2020) computations have been performed for both Mach numbers but for the 10-degree case only. The instantaneous flow field allows to identify qualitatively the spatial organisation of the coherent structures in the turbulent flow. The plot of an isosurface of the dimensionless $Q^*$ criterion represented in figure 15 permits to evidence the wide variety of turbulent scales populating the flow. In the engine bay area, a separation occurs on each nozzle leading to the development of shear layers that grow with vortex pairings. Then, fully three-dimensional structures form which look like hairpins developing in turbulent boundary layers. The flow reattaches on the main central body before encountering the grid fins. One can note in Figure 15(h) that the shock waves tend to confine the structures near the wall for the M194 case which is not the case for the transonic M08 configuration. Such an observation could explain the significant wavelength associated to the structures generated from the nozzles that can be seen for the supersonic case whereas for the transonic case these structures rapidly become fully three-dimensional.

## 7. Conclusion and future works

A sub-scale Reusable Launch Vehicle model has been numerically investigated for transonic and supersonic Mach numbers (i.e. $M_\infty$ = 0.8 and 1.94) without and with an angle of attack equal to 10°. Such a simulation has been achieved taking advantage of a multi-fidelity strategy using a ZIBC workflow which is based on the coupling between URANS or ZDES and a zonal use of IBC.
In particular, the URANS approach has permitted to categorize the main flow phenomena around the launcher and to relate them to classical academic cases for two representative flow conditions in the transonic and supersonic regimes. Then, the spatial organisation of the instantaneous flowfield for the two Mach numbers of interest has been compared. This first glimpse into the flow was a mandatory step to evidence a long wavelength in the flow associated to very long coherent structures for the supersonic case starting from the engine bay and ending in the grid fins area which is not observed in the transonic case.
In future work, the spectral content of the fluctuating field will be investigated to evidence the characteristic wavelengths of the main unsteady phenomena occurring in this massively separated flow and compared with the available experimental database.

## 8. Acknowledgments

## References

[1] L. Cambier, S. Heib, and S. Plot. The Onera elsA CFD Software: Input from Research and Feedback from Industry. *Mechanics and Industry*, 14(3):159,174, 2013.

[2] D. Charbonnier, J. Vos, A. Marwege, and C. Hantz. Computational fluid dynamics investigations of aerodynamic control surfaces of a vertical landing configuration. *CEAS Space Journal*, March 2022.

[3] L. Charrier, M. Jubera, G. Pont, F. Grasso, S. Marié, and P. Brenner. Simulations of reactive supersonic/subsonic flow interactions for space launcher applications on FLUSEPA solver. *51st International Conference on Applied Aerodynamics, Strasbourg, France, 4 - 6 April*, 2016.

[4] S. David and S. Radulovic. Prediction of buffet loads on the Ariane 5 afterbody. *6th International Symposium on Launcher Technologies, Munich, Germany, November*, 2005.

[5] A. Patureau de Mirand, J.-M. Bahu, and O. Gogdet. Ariane Next, a vision for the next generation of Ariane Launchers. *Acta Astronautica*, 170:735–749, May 2020.

[6] S. Deck. Zonal-Detached-Eddy Simulation of the flow around a high-lift configuration. *AIAA Journal*, 43(11):2372–2384, November 2005.

TOWARDS A NUMERICAL MULTI-FIDELITY STRATEGY FOR UNSTEADY AERODYNAMICS STUDIES OF
REUSABLE LAUNCH VEHICLES: APPLICATION TO ARIANE NEXT

[7] S. Deck. Recent improvements in the Zonal Detached Eddy Simulation (ZDES) formulation. *Theoretical and Computational Fluid Dynamics*, 26(6):523–550, December 2012.

[8] S. Deck and N. Renard. Towards an enhanced protection of attached boundary layers in hybrid RANS/LES methods. *Journal of Computational Physics*, 400:108970, January 2020.

[9] S. Deck and P. Thorigny. Unsteadiness of an axisymmetric separating-reattaching flow. *Physics of Fluids*, 19(065103), 2007.

[10] E. A. Fadlun, R. Verzicco, P. Orlandi, and J. Mohd-Yusof. Combined Immersed-Boundary/Finite-Difference Methods for Three-Dimensional Complex Flow Simulations. *Journal of Computational Physics*, 161(1):35–60, 2000.

[11] E. G. M. Geurts. Steady and unsteady pressure measurements on the rear section of various configurations of the ariane 5 launch vehicle. *6th International Symposium on Launcher Technologies, Munich, Germany, November*, 2005.

[12] D. Goldstein, R. Handler, and L. Sirovich. Modeling a no-slip flow boundary with an external force field. *Journal of Computational Physics*, 105(2):354–366, 1993.

[13] P. Guillen and M. Dormieux. Design of a 3D multi-domain Euler code. In *International Seminar of Supercomputing*, Boston, USA, 1989.

[14] M.C. Lai and C.S. Peskin. An Immersed Boundary Method with Formal Second-Order Accuracy and Reduced Numerical Viscosity. *Journal of Computational Physics*, 160(2):705–719, 2000.

[15] M. Laureti and S. Karl. Aerothermal databases and load predictions for retro propulsion-assisted launch vehicles (RETALT). *CEAS Space Journal*, January 2022.

[16] L. Manueco, P.-E. Weiss, and S. Deck. Towards the Prediction of Fluctuating Wall Quantities Using Immersed Boundary Conditions. *AIAA Aviation, Dallas, USA, 17-21 June*, 2019.

[17] L. Manueco, P.-E. Weiss, and S. Deck. On the estimation of unsteady aerodynamic forces and wall spectral content with immersed boundary conditions. *Computers & Fluids*, 201:104471, April 2020.

[18] A. Marwege, C. Hantz, D. Kirchheck, J. Klevanski, A. Gülhan, D. Charbonnier, and J. Vos. Wind tunnel experiments of interstage segments used for aerodynamic control of retro-propulsion assisted landing vehicles. *CEAS Space Journal*, February 2022.

[19] R. Mittal and G. Iaccarino. Immersed boundary methods. *Annual Review of Fluid Mechanics*, 37:239–261, 2005.

[20] L. Mochel, P.-E. Weiss, and S. Deck. Zonal Immersed Boundary Conditions: Application to a high Reynolds number afterbody flow. *AIAA Journal*, 52(12):2782–2794, 2014.

[21] J. Mohd-Yusof. Combined immersed-boundary/b-spline methods for simulations of flows in complex geometries. *Annual Research Briefs, Center for Turbulence Research*, pages 317–328, 1997.

[22] J. O'Rourke. Computational geometry in C, Second Edition. Cambridge University Press, 1998.

[23] R. Pain, P.-E. Weiss, and S. Deck. Zonal Detached Eddy Simulation of the flow around a simplified launcher afterbody. *AIAA Journal*, 52:1967–1979, 2014.

[24] M. Péchier, P. Guillen, and R. Caysac. Magnus effect over finned projectiles. *AIAA Journal of Spacecraft and Rockets*, 38(4):542–549, 2001.

[25] C.S. Peskin. Flow Patterns Around Heart Valves: A Numerical Method. *Journal of Computational Physics*, 10(2):252–271, 1972.

[26] C.S. Peskin. The fluid dynamics of heart valves: Experimental, theoretical and computational methods. *Annual Review of Fluid Mechanics*, 14(1):235–259, 1982.

[27] D. Saile, V. Kühl, and A. Gülhan. On the subsonic near-wake of a space launcher configuration without jet. *Experiments in Fluids*, 60(4), March 2019.

[28] R. Schwane. Numerical prediction and experimental validation of unsteady loads on ARIANE5 and VEGA. *Journal of Spacecraft and Rockets*, 52(1):54–62, January 2015.

[29] P. R. Spalart and S. R. Allmaras. A one equation turbulence model for aerodynamics flows. *La Recherche Aérospatiale*, (1):5–21, 1994.

[30] R. Verzicco, J. Mohd-Yusof, P. Orlandi, and D. Haworth. Large eddy simulation in complex geometric configurations using boundary body forces. *AIAA Journal*, 38(3):427–433, 2000.

[31] P.-E. Weiss and S. Deck. Control of the antisymmetric mode ($m = 1$) for high Reynolds axisymmetric turbulent separating/reattaching flows. *Physics of Fluids*, 23(095102), 2011.

[32] P.-E. Weiss and S. Deck. On the coupling of a zonal body-fitted/immersed boundary method with ZDES: Application to the interactions on a realistic space launcher afterbody flow. *Computers & Fluids*, 176:338–352, 2018.

[33] P.-E. Weiss and S. Deck. ZDES of an Ariane 6 PPH configuration with incidence angle using Zonal Immersed Boundary Conditions. *8th European Conference for Aerospace Sciences, Flight Physics, Launcher Aerodynamics*, 2019.

[34] P.-E. Weiss, S. Deck, J.-C. Robinet, and P. Sagaut. On the dynamics of axisymmetric turbulent separating/reattaching flows. *Physics of Fluids*, 21:075103, 2009.